# SHIPBORNE UNDERWATER–LIDAR SETUP FOR SOUNDING OF THE UPPER LAYER OF AN OCEAN

**O.A. Bukin,V.I. Il'ichev, A.Yu. Maior, A.N. Pavlov, A.G. Stafievskii, and V.A. Tyapkin**

*Pacific Oceanografic Institute,*
*Far–Eastern Branch of the Russian Academy of Sciences, Vladivostok*
*Received April 6, 1994*

*Description of the underwater–lidar setup located inside hydrooptical trunk of a research ship is presented. The design of the lidar excepts the influence of the sea surface on the results of sounding of the upper layer of an ocean and makes it possible to perform the measurements while running. The results of the measurements of the spatiotemporal structure of the laser–radiation extinction coefficient inside the ocean upper layer are presented.*

In the majority of papers on research of ocean upper layer (OUL) with laser the data on parameters of sea surface or OUL features for case of sounding through the sea surface are presented. The main advantage of sounding through the sea surface is the feasibility of measurements over large water area during the short period of time (for instance, when lidar is mounted in aircraft). It is necessary when large–scale oceanic formations are investigated or when searching work is performed. In this case there are some limitations on using such a method, which are connected with influence of the sea surface on sounding results.

This influence shows up first as the increase in intensity dispersion of backscattering signal that comes from under the surface; second, in presence of strong signal reflected from the interface (glint). The increase in intensity dispersion of backscattering signal leads to masking the signal variations, which are caused by modulation of distribution of laser extinction coefficient in depth $e(h)$ by hydrophysical structure, biomass, or dynamical processes occurring in OUL. This results in low sensitivity of the method. The reflected signal causes appearing the afterpulse of significant amplitude monitored with detecting photomultipliers. Hence, the possible sounding depth decreases and distortion of the backscattering signal shape is observed.[1] The shipborne lidar systems developed at Pacific Oceanografic Institute enable us to perform determination of feasibility of laser sounding through the sea surface under natural conditions.[1,2,3] So, in absence of ripples we were able to record the internal waves several meters in amplitude. Besides, the processes of biomass sinking in the morning were recorded as well. These processes substantially modulate the $e(h)$ function. More precise measurements, for instance, recording $e(h)$ stratification caused by distribution of hydrophysical parameters in depth or internal waves about 1 m in amplitude were impossible in our experiments.

When using immersing portholes, the influence of the surface conditions on sounding results was excepted and observation of the $e(h, t)$ spatiotemporal structures caused by distribution of hydrophysical parameters in depth as well as record of low–amplitude internal waves were found to be possible.[4] Experiments with immersing portholes can be performed only under drift or slow–running conditions. This essentially limits the operating period of an expedition. To solve this problem an underwater lidar providing laser sounding of OUL while running was designed and mounted inside the hydrooptical trunk of the *Akademik Lavrent'ev* research ship. The block–diagram of underwater lidar is presented in Fig. 1.

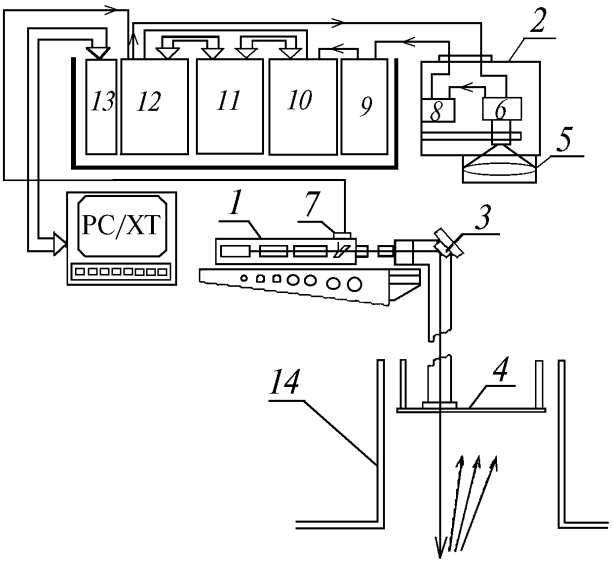


*FIG. 1. Block–diagram of the lidar located in the hydrooptical trunk of the ship. Depicted in the figure are: laser emitter (1); receiving unit (2); turning mirror (3); porthole (4); receiving objective (5); photomultipliers (6); photodiode (7); preamplifiers (8); amplifier (9); analog–to–digital converters (10, 11); control unit for electronic part of the lidar system (12); computer interface (13); and, hydrooptical trunk (14).*

The optical system for radiation transmission and recording is designed as a telescopic tube system with a porthole at the bottom. There is a sounding channel inside the tubes of large diameter. Such a system enables one to shield the detector from the sounding radiation and glint return from the porthole glass. Laser beam (emitter *1*) are directed into the water with a turning

0235-6880/94/10 761-03 $02.00 

mirror *3* and a porthole *4*. The backscattered radiation is collected with a receiver *2*. Signals from photomultipliers *6* arrive at preamplifiers and then at signal processing unit designed in CAMAC standard. Treated digital signals are input into a computer, and depth profile $e(h)$ are reconstructed. The spatiotemporal structure of $e(h)$ is screened with a color graphic monitor. Specifications of the underwater lidar are listed below.

| | |
|---|---|
| Laser wavelength | 532 nm |
| Energy per pulse | 180 mJ |
| Pulse duration | 10 ns |
| Pulse repetition frequency | up to 12 Hz |
| Receiving–objective diameter | 300 mm |
| The number of recording channels (PhÉU–79 photomultipliers) | 2 |
| Minimum depth resolution | 1.2 m |

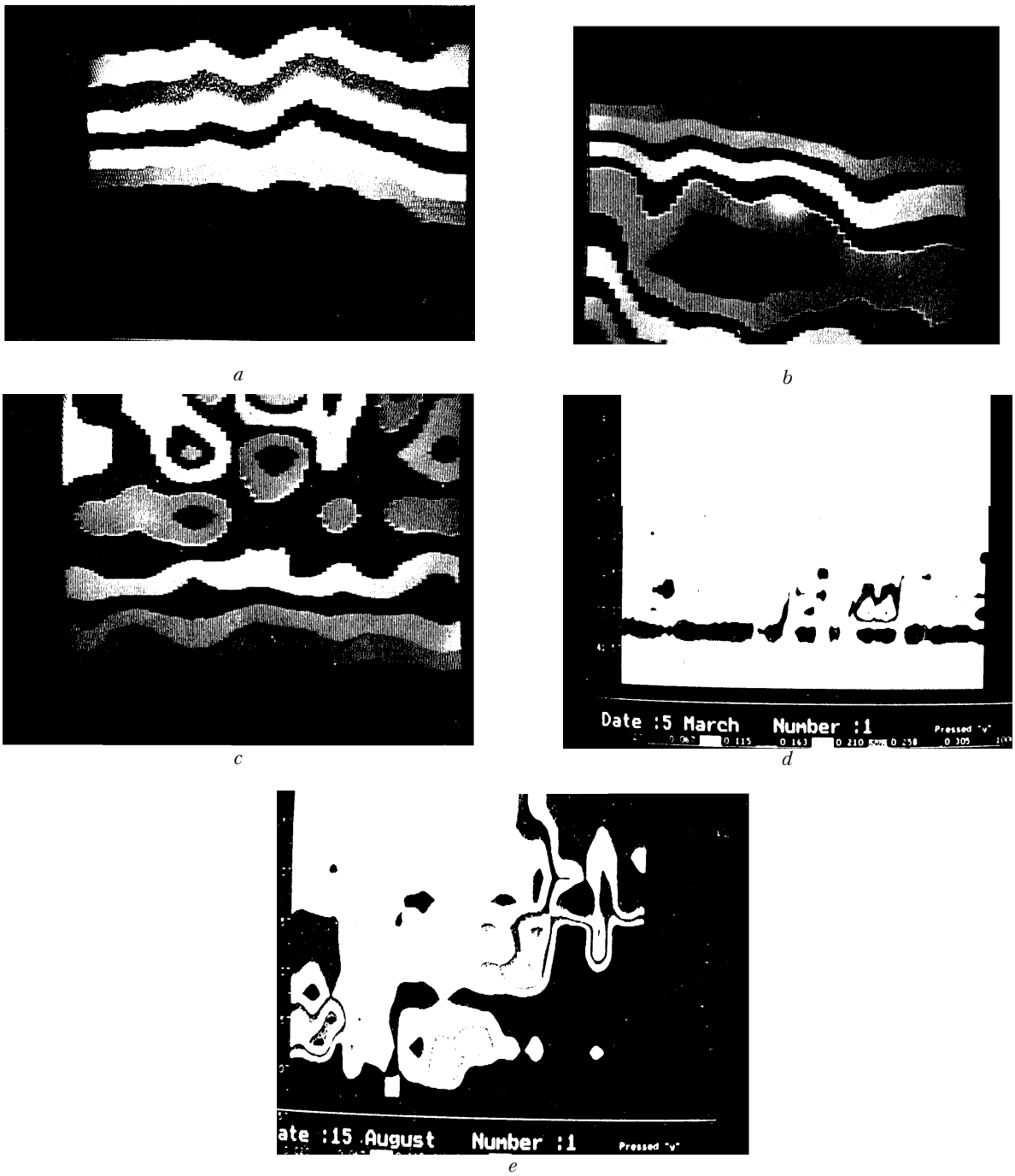


*a* *b* *c* *d* *e*

*FIG. 2. Spatiotemporal distribution of $e(h, t)$ in various underwater situations.*

The use of two recording channels enables one to match the dynamic ranges of the receiving photomultipliers and signal due to recording the signal from specified depth range with corresponding

photomultiplier. This is achieved by means of special apertures placed on photocathodes and due to sensitivity control of the photomultipliers. Joining of the results obtained with each channel is performed at the stage of signal processing and depth profile $e(h)$ reconstruction.

The design of underwater lidar allowed us to perform measurements of $e(h)$ spatiotemporal structure both while drifting and while running (the maximum speed of a ship, that did not lead to the formation of turbulent flows on the output porthole surface, was about 12 knots). The sounding beam entered the field of view of receiving objective from the points offset by 4 m from the porthole onward. Pulse fully entered the field of view at the depth of 10 m. When measuring while running, the pulse repetition frequency did not exceed 1 Hz. Different signal storage was used for depth profile reconstruction. The 10–pulse storage was carried out when operating at the maximum depth.

The small–angular approximation method was employed for $e(h)$ calculation for the depth values up to 80 m. For depth values up to 30 m we used the Monte Carlo method as well, that has provided $e(h, t)$ structure coinciding qualitatively with the spatiotemporal distribution derived with the small–angular approximation. The values of laser radiation extinction coefficient were displayed with eight colors. Thus, the continuous depth distribution $e(h)$ was presented as a layer structure. Spatiotemporal distribution of $e(h, t)$ in various underwater situations is shown in Figs. 2 *a–c*. Time varying within about one hour is plotted on the horizontal axis, and depth varying from 10 to 50 m is plotted on the vertical one. For $e(h, t)$ distributions presented in Figs. 2 *a–c* we revealed, from data on underwater measurements, the presence of seasonal thermal wedge in the range of sounded depths with different temperature lapse rate.

Figure 2 *a* shows that the boundaries of the thermal wedge were located at the depths of 15 and 24 m, whereas for $e(h, t)$ distributions indicated in Fig. 2 *b* and *c* the upper and lower boundaries were located at the depths of 17–40 and 12–50 m, respectively. The absolute temperature variations in the jump layer were approximately the same in each case. Figs. 2 *a–c* are arranged in order of decreasing of temperature lapse rate.

In the case of low temperature lapse rate (Fig. 2 *c*) we observed the formations of the transmission "lens" type, that is, the areas with low extinction coefficient and the "lens" with large $e(h)$ values. The transmission "lens" correspond to the light areas at the bottom of Fig. 2 *c*, whereas the "lens" with large $e(h)$ values correspond to dark ones. These lenses are apparently associated with the thermohaline structure of the sea water at these depths.

It should be noted that the interpretation of the $e(h)$ distribution presented here is related to specific underwater situations. However, comparative analysis of data of the lidar sounding of OUL obtained during two expeditions in 1989–1990 with those of underwater sounding demonstrated that the layers with large $e(h)$ values were detected within the depth range characteristic for thermal wedge. Values of temperature lapse rate within the thermal–wedge boundaries well correlated with values of $e(h)$ lapse rate obtained from lidar sounding data.

The image of active biomass layer observed by laser sounding while running is shown in Fig. 2 *d*. The layer is located at depth of about 40 m, the distance of about 3 miles is plotted on the horizontal axis, the depth range from 20 to 45 m is plotted on the vertical one. Identification of this layer as a biomass one was made according to its sinking in the morning.

Fig. 2 *e* illustrates potentialities of underwater–lidar system for long–path operation. The depth is plotted on the vertical axis (10–40 meters) and the distance covered by a ship on the path (~2000 miles) is plotted on the horizontal axis. The measurements were carried out continuously from 8.00 p.m. till 7.00 a.m. of the next day. The ship hull shielded partially solar background, hence we were able to perform sounding in the morning and evening hours at the depth up to 40 m. Data obtained over previous day were joined with the results of following measurements. Thus, the continuous picture of the spatiotemporal distribution was reconstructed.

The above–presented results demonstrate the potentialities of shipborne underwater–lidar system. Even a provisional analysis of the obtained data shows that the spatiotemporal structure of $e(h, t)$ reconstructed in such a manner can be used for investigation into the processes in OUL, for instance, examination of streams, frontal zones, internal waves. The maximum depth of $e(h, t)$ reconstruction was found to be about 80 m. This value is limited by the lack of reliable algorithms for calculation of the extinction coefficient in the case of large optical thickness.

The operation of the underwater–lidar setup and the method of information representing are similar to specific features of acoustic sounding systems in many respects. Therefore, the correlation analysis of the data obtained by optical and acoustic sounding seems to be easy. The simultaneous optical and acoustic sounding makes it possible to remove the uncertainty of process identification in OUL.

## ACKNOWLEDGMENTS

In conclusion the authors would like to thank S.A. Kharchenko for design of underwater–lidar system.

## REFERENCES

1. O.A. Bukin, V.D. Kiselev, S.A. Klenin, et al., "*Integrated optical and acoustic sounding of the ocean upper layer*", Pacific Oceanografic Institute of the Far–Eastern Branch of the Academy of Sciences of the USSR, Vladivostok (1988), 18 pp.
2. V.I. Il'ichev, O.A. Bukin, V.N. Lysun, et al., Dokl. Akad. Nauk SSSR **303**, No. 6, 1482–1485 (1988).
3. V.I. Il'ichev, O.A. Bukin, V.N. Lysun, et al., Pacific Ocean Annual, 185–190 (1988).
4. O.A. Bukin, V.I. Il'ichev, I.A. Kritskii, and A.N. Pavlov, Dokl. Akad. Nauk SSSR **312**, No. 4, 972–973 (1990).